Insoluble γ-Tubulin–containing Structures Are Anchored to the Apical Network of Intermediate Filaments in Polarized CACO-2 Epithelial Cells

Pedro J.I. Salas

University of Miami School of Medicine, Department of Cell Biology and Anatomy, Miami, Florida 33101

Abstract. We have previously shown that a thin (~1 μm) layer of intermediate filaments located beneath the apical membrane of a variety of simple epithelial cells participates in the organization of apical microfilaments and microtubules. Here, I confirmed the apical distribution of γ-tubulin–containing structures (potential microtubule-organizing centers) in CACO-2 cells and demonstrated perfect colocalization of centrosomes and nearly 50% of noncentrosomal γ-tubulin with apical intermediate filaments, but not with apical F-actin. Furthermore, the antisense-oligonucleotide–mediated downregulation of cytokeratin 19, using two different antisense sequences, was more efficient than anticytoskeletal agents to delocalize centrosomes. Electron microscopy colocalization suggests that binding occurs at the outer boundary of the pericentriolar material. Type I cytokeratins 18 and 19 present in these cells specifically coimmunoprecipitated in multi-protein fragments of the cytoskeleton with γ-tubulin. The size and shape of the fragments, visualized at the EM level, indicate that physical trapping is an unlikely explanation for this result. Drastic changes in the extraction protocol did not affect coimmunoprecipitation. These results from three independent techniques, indicate that insoluble γ-tubulin–containing structures are attached to apical intermediate filaments.

Key words: cell polarity • centrosome • γ-tubulin • intermediate filaments • keratin

Epithelial polarity, the ability of simple epithelial cells to become asymmetric, with distinct apical and basolateral domains in the plasma membrane, is a puzzling, as yet unsolved case of how cells can generate different subdomains. There is a consensus that epithelial cells sort out newly synthesized membrane proteins at the trans-Golgi network (Rodriguez-Boulan and Nelson, 1989; Simons and Wandinger-Ness, 1990) and recycled membrane proteins at an intermediate endosomal compartment (Mostov, 1995). The vesicular traffic originating from these sorting compartments is probably directed by cytoskeletal components to their final destinations in the apical or basolateral domains and retained in place (Wollner and Nelson, 1992).

Although epithelial cells can deliver polarized proteins without organized microtubules (Salas et al., 1986; Grindstaff et al., 1998), several lines of evidence support the idea that microtubule based motors participate in the movement of exocytic vesicles at least along part of their pathway (Lafont et al., 1994). Moreover, in well-differentiated simple epithelia, microtubules are organized in the apico-basal axis with their minus ends toward the apical side (Troutt and Burnside, 1988; Bacallao et al., 1989; Redenbach and Vogl, 1991). This organization is thought to participate in the polarization of organelles in the cytoplasm and to contribute to the polarized vesicular traffic. This peculiar arrangement of the microtubules must result from a polarized distribution of microtubule organizing centers (MTOC)[1] under the apical domain. In fact, centrosomal structures distribute under the apical membrane in a number of simple epithelium cells in interphase, both ciliated and nonciliated (Buendia et al., 1990; Rizzolo and Joshi, 1993; Apodaca et al., 1994; Meads and Schroer, 1995). Interestingly, when epithelial cells enter mitosis, the centrosomes move toward the lateral domains, organizing the mitotic spindle always perpendicular to the apico-basal axis, and then move back to the apical domain when the cells complete mitosis (Reinsch and Karsenti, 1994). The significance of this elaborate redistribution of centrosomes is currently unknown. It is especially intriguing since

Address correspondence to Pedro J.I. Salas, University of Miami School of Medicine, Department of Cell Biology and Anatomy, R-124, P.O. Box 016960, Miami, FL 33101. Tel.: (305) 243-6977. Fax: (305) 545-7166. E-mail: psalas@mednet.med.miami.edu

1. *Abbreviations used in this paper:* CK, cytokeratin; EB, extraction buffer (PBS, 2 mM EDTA, 1% Triton X-100); IF, intermediate filaments; i.p., immunoprecipitation; KEB, extraction buffer (70 mM KCl, 80 mM Pipes, pH 6.5, 5 mM EGTA, 2 mM $MgCl_2$, 0.1% saponin); MTOC, microtubule-organizing center.

Meads and Schroer (1995) demonstrated that, while apical (interphasic) centrosomes retain their capability to act as MTOC, most of the microtubules are organized by noncentrosomal MTOCs, diffusely distributed under the apical domain.

In previous studies we found that a network of intermediate filaments (IF) underlying the apical membrane of epithelial cells contains cytokeratin (CK) 19 IF, which are attached to a subpopulation of apical membrane proteins (Rodriguez et al., 1994). Furthermore, this IF network, equivalent to the terminal web, was observed in a variety of epithelial cells with or without brush-border. Using antisense oligonucleotides, we could transiently downregulate CK19 in a fraction of CACO-2 epithelial cells. Those cells displayed a characteristic phenotype, with abolished apical F-actin (while the rest of cortical F-actin was normal), distinctive changes in the polarization of membrane proteins, and disorganization of the apical, but not basal, network of microtubules (Salas et al., 1997). The latter observation, together with the reports of an apical distribution of MTOC mentioned above, prompted us to hypothesize that the apical IF may be responsible for the polarized distribution of γ-tubulin–containing structures in simple epithelia. It is generally accepted that γ-tubulin is an essential component of MTOC (Oakley et al., 1990; Stearns et al., 1991; Archer and Solomon, 1994; Joshi, 1994). It remains associated with the centrosomes even when the microtubules are depolymerized (Stearns et al., 1991). Approximately 50% of the γ-tubulin is in a soluble form, part of a 28S complex, while the rest is insoluble, presumably associated with centrosomes (Stearns and Kirschner, 1994). Therefore, the possibility of binding of MTOC to apical IF was analyzed, by studying the attachment of insoluble γ-tubulin to CKs. The results indicate that apical IF comprising CKs19-8 and CKs18-8 are sites of attachment of γ-tubulin–containing structures. These findings suggest that IF may occupy a higher place than previously suspected in the hierarchy of organization of the cytoskeleton in epithelial cells.

Material and Methods

Antibodies and Oligonucleotides

The primary specific antibodies used in this study were: mAb anti-CK19 (RCK 108) (Accurate Chemical & Scientific Corp.); mAb anti-CK18 (B23.1) (Biomeda Corp.); mAb anti-CK8 (B22.1) (Biomeda Corp.); rabbit polyclonal antibody against a synthetic polypeptide comprising amino acids 38-53 (EEFATEGTDRKDVFFY) of the NH_2-terminal region of human γ-tubulin (Sigma Chemical Co.); mAb against the same synthetic peptide of human γ-tubulin (Accurate Chem. & Scientific Corp.); mAb against α-tubulin (DM 1A) (Sigma Chemical Co.); and mAb against all actin isoforms (C4) (ICN Biomedicals Inc.). All secondary antibodies were affinity-purified and had no cross-reactivities with immunoglobulins of other species (Jackson ImmunoResearch Laboratories). F-actin was labeled with FITC-phalloidin (Molecular Probes). Low molecular mass Fab goat anti–rabbit IgG coupled to peroxidase was purchased from Protos Immunoresearch.

Synthetic phosphorothioate oligodeoxy nucleotides have been used extensively to reduce the synthesis of specific proteins. Four 21-mer oligonucleotides, two with antisense sequences for CK19 mRNA (A19: 3′-TACTGAAGGATGTCGATAGCG, and A19/2: 3′-AGGAAGTCATGGCGAGGCGGA) and their corresponding scrambled sequences (random: 3′-GAAGCTATTGAGACTGGGATC and random/2: 3′-GGGAGAAGAGTGGTGCCGAAC) were synthesized and extensively purified as described before (Salas et al., 1997).

Cell Culture and Treatments

CACO-2 cells (clone C2BBe1; CRL-2102) were obtained from American Type Culture Collection and grown in flasks, 24-mm or 6-mm Transwell-Clear™ filters (for experiments), or roller bottles (Corning Costar) as described before (Salas et al., 1997). For experiments with anticytoskeletal agents, the cells, at 9 d after seeding, were incubated in DME-F12 supplemented with 33 μM nocodazole, 2 μM cytochalasin D, or 5 mM acrylamide (all from Sigma Chemical Co.) for 7 h before fixation or extraction. Metabolic labeling was performed with 0.15 mCi/ml [^{35}S]methionine and [^{35}S]cysteine (EXPRE Protein Labeling Mix; NEN) in DME with only 15 μM methionine and cysteine for 24 h. For antisense downregulation, cells were maintained in the standard tissue culture media containing 2–10 μM phosphorothioate oligonucleotides as described before (Salas et al., 1997).

Double Immunofluorescence, Confocal Microscopy, Image Analysis, and Immunoelectron Microscopy

Immunofluorescence procedures were described as before (Vega-Salas et al., 1987a,b). The cells were fixed in 100% methanol at −20°C. We have previously demonstrated that the morphology of the apical IF cytoskeleton is similar under methanol, formaldehyde or formaldehyde/glutaraldehyde fixations (Salas et al., 1997). Likewise, Stearns et al. (1991) has shown that the method of fixation does not affect the localization of γ-tubulin. Double indirect immunofluorescence was performed using a monoclonal antibody against CK19 and a rabbit polyclonal antibody against γ-tubulin together, and two secondary antibodies raised in goats with no cross-reactivity, and labeled with FITC (anti-rabbit) or CY3 (anti-mouse). Transwell™ filters holding the cell monolayers were mounted in polyvinyl alcohol as described before (Salas et al., 1997).

Laser confocal microscopy was performed with an Odyssey XL (Noran Instruments) microscope, using an Omnichrome laser source. For colocalization experiments (FITC/CY3), a second detection channel was used separating the light with a custom made 540 nm secondary dichroic using a 565 LP emission filter in the red channel and a 535 ± 20 nm emission filter in the green channel (all from Omega Optical Inc.). To increase resolution in the z-axis, a 15-μm slit was routinely used. The images were collected using Intervision software (Noran Instruments). Each confocal section was obtained as the average of 32 frames to filter noise. The sections were collected at 0.3-μm intervals in the z-axis for low magnification images comprising the entire thickness of the monolayer or at 0.1-μm intervals for high-resolution imaging of the apical domain with 100-nm pixels (nearly cubic voxels for high resolution images) through a 63× oil immersion objective. Usually, each field comprised 60–90 confocal sections. Before three-dimensional reconstruction, the images were subjected to three-dimensional deconvolution using Intervision software for nine neighboring voxels. Convergence was usually achieved at or before 10 iterations. To experimentally adjust the parameters of the deconvolution, test the coalignment of the channels, and assess the final limit of resolution of the system after deconvolution, single or double fluorescent 1-μm beads (Molecular Probes) were used. To adjust the point spread function parameter, the same confocal stacks from preparations in the standard mounting medium were processed using different parameters until the distortion in the z-axis was abolished. Three-dimensional reconstructions were performed using Intervision software on deconvoluted stacks of confocal images. Pixel intensity histograms over single cell areas were used to assess efficiency of the antisense targeting. For z-sections (perpendicular to the plane of the monolayer), the deconvoluted images were cut in 9-pixel-thick volumes (in the x-axis) at the desired level, reconstructed, and rotated 90° to obtain a view of the apico-basal axis.

For immunolocalization at the EM level, we combined the procedures of Nanogold™ (Nanoprobes, Inc.) and immunoperoxidase for EM (Brown and Farquhar, 1984). Both first antibodies (mAb anti-CK19 and rabbit anti–γ-tubulin) were added together. To avoid interactions between the peroxidase and the silver enhancer of Nanogold, we completed all the steps of the Nanogold procedure first, and then incubated the cells with the Fab anti–rabbit IgG-peroxidase and followed the diaminobenzidine reaction as described before (Vega-Salas et al., 1987b).

Cytoskeletal and Cytokeratin Preparations, Gradient Separation of Cytoskeletal Fragments

Cytoskeletal preparations were obtained as described before (Salas et al., 1988). In brief, the monolayers were washed in PBS, extracted in PBS

containing 1% Triton X-100, 2 mM EDTA (extraction buffer, EB) and a cocktail of antiproteases (Sigma Chemical Co.) for 10 min at room temperature, and centrifuged for 9 min in an Eppendorf type centrifuge (14,000 rpm). Alternative extractions, in a more physiologic condition, were performed in 70 mM KCl, 80 mM Pipes (pH 6.5), 5 mM EGTA, 2 mM $MgCl_2$ supplemented with 0.1% saponin (KEB buffer), and 2 nM calciulyn, 5 μM okadaic acid, and 0.5 mM sodium orthovanadate in addition to the standard cocktail of antiproteases. Cytokeratin preparations were obtained by Triton extraction in 1.5 M KCl followed by cycles of 9 M urea solubilization and repolymerization as described by Steinert et al. (1982).

To obtain fragments of the cytoskeletal preparations, the pellets from the first centrifugation were resuspended in 1 ml EB (or KEB) in Eppendorf tubes. Then, the pellets were sonicated while immersing the tubes in ice-water for a total of 3 min (actual sonication time), with intervals of 10-s sonication (~250 watts, 5 on a scale of 10) and 15-s gaps to allow for heat dissipation. The suspensions of cytoskeletal fragments were immediately loaded on top of a preformed 10-ml continuous sucrose gradient (20–60% sucrose in EB or KEB) and centrifuged in a Beckman ultracentrifuge at 15,000 rpm for 50 min in a swinging bucket rotor (Beckman SW-40) at 4°C. The gradients were fractionated from the top by gently pipetting ten 1-ml fractions from the surface. No sedimentation standards are available for values well >100 S, except for viral particles that provide an approximate calibration for the gradient.

To determine the shape and size of the cytoskeletal fragments we used two methods: (a) 1 μl of the corresponding gradient fractions were spread on carbon-coated EM grids and stained with 2% uranyl acetate; and (b) the fractions were fixed in 2% glutaraldehyde, pelleted, embedded in Spur and sectioned. The EM samples were observed and photographed under a JEM 100-CX II (JEOL) transmission electron microscope.

Electrophoresis, Immunoprecipitation, and Immunoblot

Single dimension SDS-PAGE was performed as described by Laemmli (1970) and two-dimensional (IEF and SDS-PAGE) electrophoresis was performed as described by O'Farrell (1975). Immunoblot and nitrocellulose reprobing were performed as described before (Salas et al., 1997). For immunoprecipitation, fractions 1–5 of the gradients described above were diluted with 1 ml EB (or KEB), divided into two equal 1-ml aliquots, and one of the aliquots was mixed with a 1:100 dilution of the purified IgG polyclonal anti–γ-tubulin antibody (+ in Figs. 8 and 9), while the other was supplemented with 15 μg/ml purified nonimmune IgG (− in Figs. 8 and 9). All the samples were supplemented with 0.1% globulin-free albumin (Sigma) and incubated for 2 h with gentle rotation. Then, 10 μl of protein A–agarose beads (Pharmacia Biotech Inc.) preincubated in 0.1% albumin, were added to each sample and incubated overnight with gentle rotation at 4°C. Next, the beads were centrifuged through a 0.5-ml 30% sucrose cushion and washed four times in EB (or KEB) for 1 h each time. All centrifugations were done at 14,000 rpm for 2 s to minimize unspecific copelleting of unbound filaments. After the last wash, the beads were eluted in 1 ml 2% SDS, and 4 M urea for 2 h. The eluates were TCA precipitated and the pellets washed twice in 100% acetone at −20°C. The pellets were resuspended for 2 h in SDS sample buffer and analyzed by SDS-PAGE and immunoblot/chemiluminescence or autoradiogram in a PhosphorImager (Molecular Dynamics).

Results

Centrosomes and Noncentrosomal γ-Tubulin Colocalize with Apical IF in CACO-2 Cells

Because CACO-2 cells undergo a complex differentiation process as they become confluent and polarized, we first determined the types of IF as a function of time after confluency. Purified IF proteins were analyzed by two-dimensional gels at 3 d (nondifferentiated, poorly polarized), 7 d (onset of the development of brush border), 9 d (brush border complete), and 15 d (fully differentiated). The CKs were essentially the same and comprised type I CKs 19 and 18, and CK8 as the only type II partner available (Fig. 1). Therefore, CACO-2 cells express IF composed of pairs CK18-CK8 and CK19-CK8 at all the stages of differentiation. For the sake of brevity, these IF will be referred to as CK18 or CK19, respectively, hereafter, and were identified with specific monoclonal antibodies against these two type I cytokeratins.

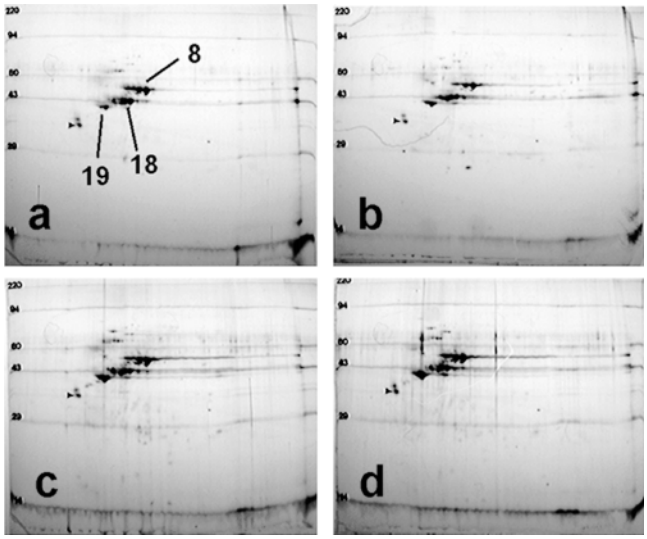

Figure 1. Expression of cytokeratins in CACO-2 cells. Purified IF proteins from CACO-2 monolayers confluent for 3 d (a), 7 d (b), 9 d (c), and 15 d (d) were separated by two-dimensional electrophoresis (IEF, first dimension and SDS-PAGE in the second dimension). Notice that only cytokeratins 8, 18, and 19 were expressed at all times. Small arrowheads point to an internal standard, tropomyosin (mol wt 33,000, pI 5.2). Molecular mass standards are given in kD.

Next, CACO-2 monolayers at the 9-d stage were fixed and analyzed by double immunofluorescence, using a polyclonal antibody against a polypeptide in the COOH-terminal region of γ-tubulin and monoclonal antibodies against CKs 18 and 19. Raw (nondeconvoluted) confocal images in the XY plane indicated that centrosomes (Fig. 2 a, green signal, arrows) were in the same confocal plane of apical IF. Noncentrosomal γ-tubulin signal was also abundant in the same plane. Low magnification XZ sections (perpendicular to the monolayer) showed a difference in the distribution of CK19 IF (Fig. 2 b) and CK18 (Fig. 2 c). The former was mostly restricted to the apical cortical cytoskeleton, with small (<1 μm) extensions into the lateral domain. The specificity of this distribution of CK19 has been tested before with a panel of four different monoclonal antibodies and one polyclonal antibody against CK19 in three different cell lines (Salas et al., 1997). CK18 signal was also present in the apical cortical region but, in addition, extended throughout the lateral cortical region and, in some cells, even under the basal domain. This result is similar to previous observations in MCF-10A mammary epithelial cells and MDCK cells (Rodriguez et al., 1994; Salas et al., 1997). In the vast majority of the cells, the centrosomes were observed in the apical domain, colocalizing with the apical cortical layer of IF (Fig. 2, b and c, arrows). In <10% of cells the centrosomes were found >0.3 μm away from the cortical IF network (Table I). These results are consistent with the findings of Karsenti and coworkers and other investigators in MDCK cells (Buendia et al., 1990; Meads and Schroer, 1995).

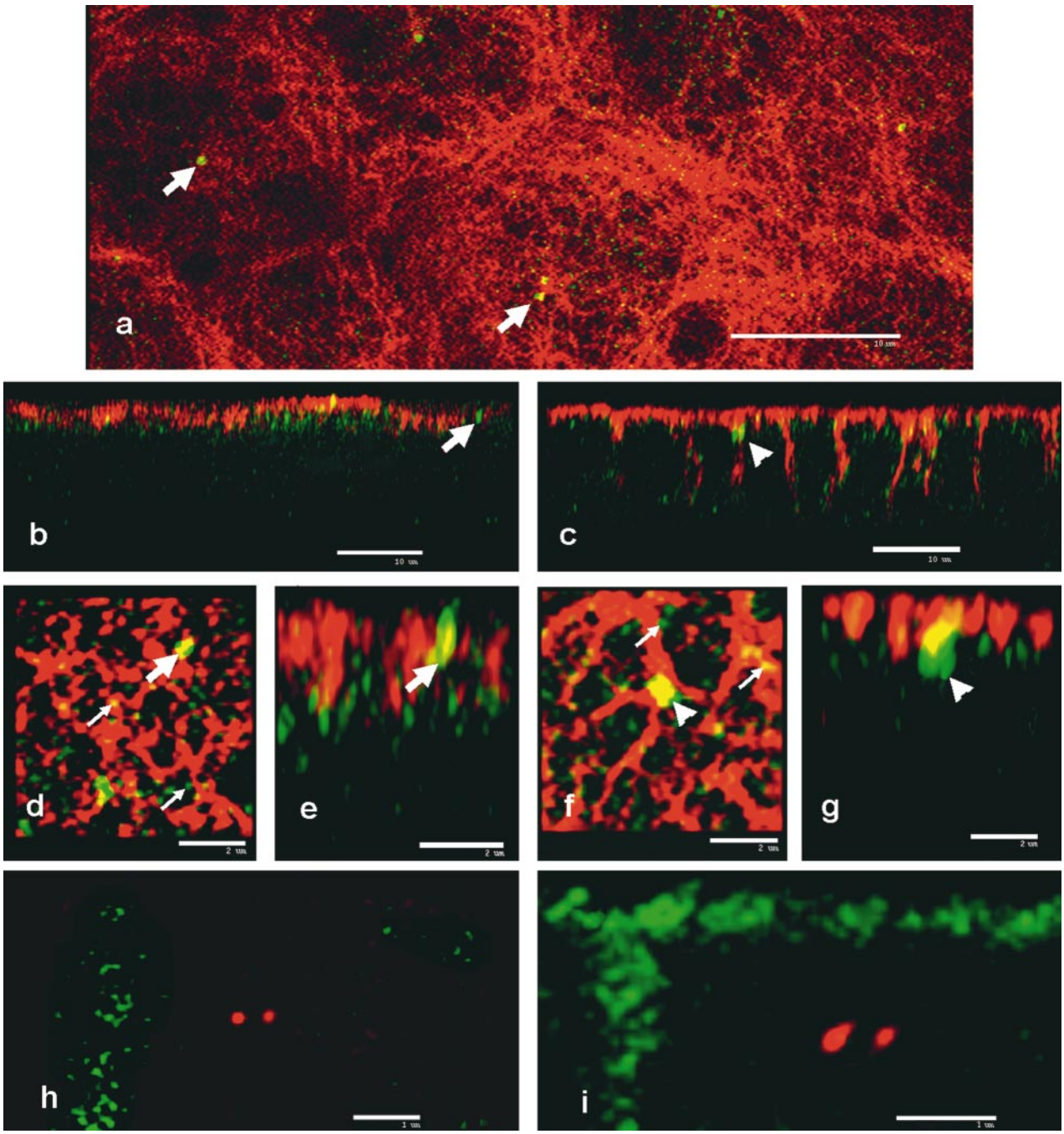

Figure 2. γ-tubulin colocalizes with apical IF but not with apical F-actin in CACO-2 cells. CACO-2 cells grown on Transwell™ filters at 9 d confluency stage were fixed and processed for double indirect immunofluorescence for γ-tubulin (green), and CK19 (b, d, and e) or CK18 (a, c, f, and g) (red). The preparations were analyzed by laser scanning confocal microscopy and the stacks of confocal sections were further subjected to three-dimensional deconvolution. a, d, and f represent confocal sections in the XY plane (parallel to the monolayer). b, c, e, and g are XZ reconstructions (perpendicular to the plane of the monolayer, apical is shown up). e is the XZ cross-section of the image in d, at the level of the arrow, while g is the XZ cross-section of the image in f, at the level of the arrowhead. Large arrows point at centrosomes and small arrows at noncentrosomal γ-tubulin spots. In h and i γ-tubulin (red) signal was colocalized with FITC-phalloidin signal (green). h represents a XY section and i represents a XZ section of the same field. Bars: (a–c) 10 μm; (d–g) 2 μm; (h and i) 1 μm.

For better resolution, the images were subjected to three-dimensional deconvolution, thus filtering minimal nonconfocal contributions of out-of-focus fluorescence. The image acquisition, the coalignment of the red and green channels, and the deconvolution parameters were calibrated using fluorescent beads. Under these conditions the image resolution approached the pixel size (~100 nm per side). Although we cannot colocalize CK19 and CK18, both types of IF displayed a similar distribution under the apical domain. The network of CK19 IF bundles was

Table I. Distribution of Centrosomes in CACO-2 Cells after Treatments that Disrupt the Cytoskeleton

Condition	% Total cells	% Centrosomes per region		
		Apical	Deep cytoplasmic*	Lateral‡
Anticytoskeletal agents				
None (control)	N/A	91	0	9
Nocodazole	N/A	98	0	2
Cytochalasin D	N/A	94	0	6
Acrylamide	N/A	67	33	0
Acrylamide reversal (24 h)	N/A	87	13	0
Anti-CK19 antisense oligonucleotides				
A19				
Nontargeted cells	39	98	0	2
Partially targeted cells	54	36	36	28
Fully targeted cells	7	0	56	44
A19/2				
Nontargeted cells	36	92	0	8
Partially targeted cells	62	41	33	26
Fully targeted cells	2	0	50	50

CACO-2 cells (9 d stage) were either treated with anticytoskeletal agents for 7 h (33 μM nocodazole, 2 μM cytochalasin D, or 5 mM acrylamide) in DME, treated with 5 mM acrylamide for 7 h and then incubated in DME for 24 h (acrylamide reversal), and fixed, or treated with anti-CK19 antisense oligonucleotide for at least three passages. Centrosomes were counted in three-dimensional confocal deconvoluted images from colocalizations of CK19 or CK18 and γ-tubulin as those shown in Figs. 2 and 3. The data from two independent experiments, counting 66 cells are shown as percent of centrosomes in the apical, deep cytoplasmic or lateral domains. For apical or lateral localization centrosomes at <0.3 μm of the corresponding domain of cortical CK19 signal were counted.

*Deep cytoplasmic centrosomes were counted as those located at >0.3 μm below the boundary of the apical IF network (limit of resolution in the z-axis).

‡Lateral localization could only be assessed by colocalizations with CK18 (top part of the table). In colocalizations with CK19 (bottom part of the table), lateral was defined as immediate vicinity to a neighbor nontargeted cell. In the antisense oligonucleotide part of the experiments, nontargeted cells were used as an internal control for morphologic experiments. Cells treated with the scrambled oligonucleotides showed distributions similar to nontreated controls. Partially targeted cells were those showing a substantial decrease (arbitrarily defined as those showing <50% of maximum signal in nontargeted cells in three-dimensional projections such as those shown in Fig. 3, a–c) in the CK19 signal as determined in area histograms of pixel intensities (e.g., Fig. 3, b and c, arrows). Fully targeted cells were those in which <10% of maximum CK19 signal was detectable in the entire cell (e.g., Fig. 3 a, arrow).

denser (Fig. 2 d, red signal) than its CK18 counterpart (Fig. 2 f, red signal). In both cases, the apical IF network was ~1 μm thick in the z-axis (Fig. 2, e and g). At this resolution level, centrosomes, identified as the largest (~400 nm) spots of γ-tubulin signal, often observed in pairs, were easily distinguishable (Fig. 2 d–g, arrows, green signal), and always colocalized with IF in the 3 axis of space.

The abundant noncentrosomal γ-tubulin signal under the apical domain described by Meads and Schroer (1995), was observed as discrete spots smaller (~170 nm) than centrosomes. A fraction of these spots (~40%, see Fig. 5, Control) was also perfectly colocalizing with apical IF (Fig. 2, d and f, small arrows). This colocalization was better seen in XY confocal sections than in XZ reconstructions (9 voxel thick). Most of the rest of the noncentrosomal γ-tubulin signal, however, was observed within 3 μm of the apical IF network (z-axis in the basal direction), while a few were also scattered in the rest of the cytoplasm and in the cortical region underneath the basolateral domain. At large, however, the majority of the γ-tubulin signal was observed at or underneath the apical cortical IF network (Fig. 2, b and c).

Because F-actin is also a component of the terminal web, it was important to assess whether or not the γ-tubulin signal also colocalized with apical microfilaments. In CACO-2 cells stained with FITC-phalloidin and indirect immunofluorescence for γ-tubulin (CY3), we found that 81% of the centrosomes appeared disconnected from the phalloidin signal both in XY sections (Fig. 2 h, F-actin signal corresponds to the upper lateral region), or in XZ sections (Fig. 2 i). Only 9% of the centrosomes were found colocalizing with F-actin signal at the apical domain. The centrosomes at the lateral domain (10%), on the other hand, always colocalized with cortical actin. In early experiments, we had found that, while there is a general colocalization of F-actin and IF, the microfilaments occupy mostly the apical side of the terminal web, and the CKs are the major components at the nuclear side of the terminal web (not shown). The centrosomes, therefore, usually attached to that nuclear face appeared separated from the F-actin signal.

Downregulation of CK19 with Antisense Oligonucleotides Dislodges Centrosomes in Targeted Cells

In a previous publication (Salas et al., 1997) we showed downregulation of CK19 by continuous incubation of expanding cell populations in media supplemented with 2–10 μM antisense phosphorothioate oligodeoxy nucleotides (A19 or A19/2) targeting two different sequences around the origin of the open reading frame of CK19 mRNA. Both antisense oligonucleotides gave similar results, clearly contrasting with their corresponding randomized sequences used as a control. The downregulation of CK19 is only partial and temporary, but, at day 9 of CACO-2 cells confluency is sufficient to show a phenotype. As reported before, fractions of the cells were not targeted at all (36–39%, Table I), some cells were partially downregulated (54–62%, arbitrarily defined as cells displaying <50% of maximum total CK19 signal in three-dimensional reconstructions, Table I) and some were fully targeted, not showing CK19 at all (2–7%, cells displaying <10% of maximum CK19 signal, Table I). Although some variability in the CK19 signal was observed in control monolayers (either under no treatment or incubated in parallel with random or random/2 oligonucleotides), no cells with these low levels of CK19 (<50% of maximum) were observed in the controls (see Fig. 2, i–j in Salas et al., 1997).

Examples of cells downregulated in CK19 with A19 antisense oligonucleotide are shown in Fig. 3. The top panels (a–c) in Fig. 3 are three-dimensional projections of the whole stack of confocal sections in the XY plane, and, therefore, show the total CK19 content of the entire cell. Each panel shows at least one example of a fully targeted or partially targeted cells (Fig. 3, a–c, arrows), surrounded by neighbor nontargeted cells (Fig. 3, a–c, *) shown as an internal control. Examples of partially targeted cells are shown in Fig. 3, b and c (arrows), while a fully targeted cell is shown in Fig. 3 a (arrow). To analyze the position of centrosomes in all these cells (Fig. 3, arrows and arrowheads), two XZ sections of each three-dimensional image were taken at the level of the centrosomes. The second row of panels (Fig. 3, d–f) are the XZ sections at the level

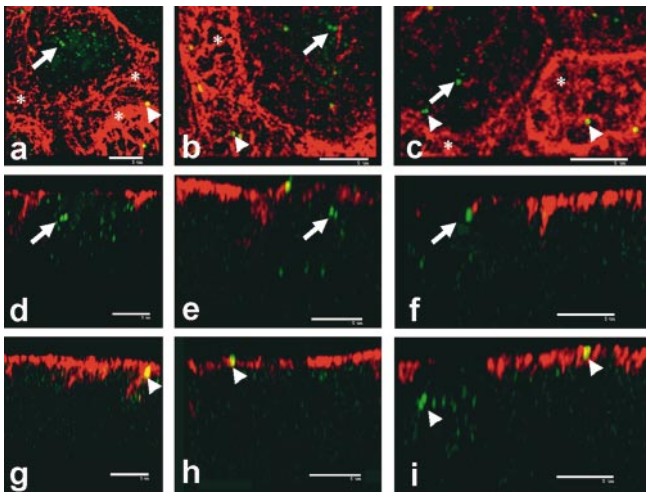

Figure 3. Redistribution of centrosomes in CACO-2 cells depleted in CK19 by antisense oligonucleotide treatment. CACO-2 cells were continuously grown on Transwell™ filters in the presence of A19 oligonucleotide. The monolayers were fixed, processed for double immunofluorescence, and analyzed by confocal microscopy and deconvolution as described in Fig. 2. a–c show different examples of cells depleted in CK19 (red signal) with neighboring nontargeted cells (*), viewed in the XY plane (parallel to the monolayer). d–i are XZ sections (apical is shown up) of the same XY image above, at the level of the arrows (d–f) or the arrowheads (g–i). Arrows and arrowheads point at centrosomes. Bars, 5 μm.

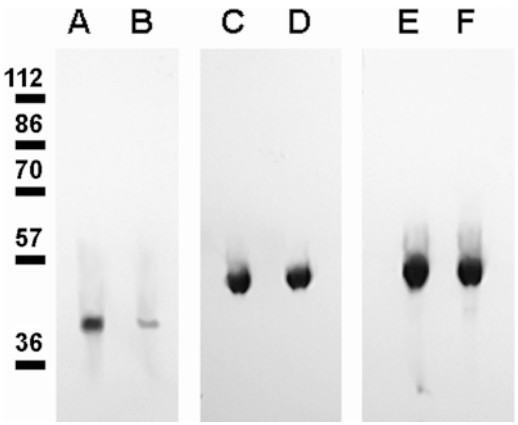

Figure 4. Effect of anti-CK19 phosphorothioate antisense oligonucleotide on steady-state levels of cytokeratins in CACO-2 cells. CACO-2 cells were continuously incubated with the phosphorothioate oligodeoxy nucleotide A19, antisense against the CK19 mRNA (b, d, and f) or R, its randomized sequence (a, c, and d), as a control, for three passages. In this experiment, the cells were grown on 24-mm Transwell™ filters, and the cytoskeletal IF preparation was obtained by extraction in Triton X-100 in the presence of 1.5 M KCl. The pellets were analyzed by immunoblot using anti-CK19 (a and b), anti-CK18 (c and d), and anti-CK8 (e and f) mAbs. Molecular mass standards are expressed in kD.

of the centrosomes pointed with arrows, while the third row (Fig. 3, g–i) are XZ sections at the level of the centrosomes pointed with arrowheads. Totally or partially targeted cells are shown in the second row (Fig. 3, d–f), while their nontargeted neighbors are shown in the third row (Fig. 3, g–i, arrowheads) with the exception of the cell on the left hand side of i. The position of the apical domain and its cortical apical network of IF was hinted in targeted cells by the few remnant IF, that, in addition, were at the same level as those clearly visible in the nontargeted neighbors. In clear contrast with the control cells or the nontargeted cells in the same monolayers treated with A19, most cells downregulated in CK19 showed centrosomes 2–3 μm below the IF network (Fig. 3, d, e, and i). In some cases, when the centrosomes were at the level of the apical IF network, they were always colocalizing with one of the remnant CK19 bundles (Fig. 3 f). Likewise, there was a correlation between the proportion of centrosomes not localized to the apical domain and the degree of success of the antisense treatment. In partially downregulated cells, 33–36% of the centrosomes were still apical, while none was found in totally downregulated cells (Table I). In all cases, however there was an increase in the proportion of centrosomes localized at the lateral boundaries of the cells (as identified by the vicinity to a neighbor nontargeted cell) (Table I). In the nontargeted cells, centrosomes were always colocalizing with the apical IF network (Fig. 3, g–i). Noncentrosomal γ-tubulin was also delocalized in cells downregulated in CK19 (Fig. 3, d, e, and i). Since half of the noncentrosomal γ-tubulin is not in direct contact with the IF, but within a 2–3-μm range, this suggests that CK19 IF may also play an indirect role in the localization of this signal to the apical pole of epithelial cells. Both 21-mer A19 and A19/2 antisense oligonucleotides showed similar results (Table I), suggesting that the probabilities that these results are due to the downregulation of other, unrelated, mRNAs are very low. In all cases, the success of antisense downregulation was checked in parallel monolayers by immunoblot. Usually, a 50–70% decrease of CK19 signal was observed (Fig. 4), while CK18, CK8 (Fig. 4) or actin (Salas et al., 1997) were not affected. Similar results were observed with A19/2 (not shown).

Acrylamide Decreases the Colocalization of Centrosomes and Noncentrosomal γ-Tubulin with IF

To dissect the molecular mechanisms connecting γ-tubulin–containing structures to apical IF, I reanalyzed the distribution of γ-tubulin in CACO-2 cells treated with anticytoskeletal agents. Nocodazole and cytochalasin D were chosen because of their well known effects on microtubules and microfilaments, respectively. Unfortunately, there is no equivalent anti-IF drug available. A toxic effect reported for IF is that of acrylamide, that does not necessarily depolymerize IF, but may rather detach them from their anchors, for example, the desmosomes (Shabana et al., 1994). In all cases, long incubations (7 h) with these agents were used to allow for redistribution of the relatively large MTOC that may have exceedingly slow diffusion rates in the cytoplasm (Luby-Phelps et al., 1987). Neither nocodazole or cytochalasin D treatments resulted in a noticeable delocalization of apical centrosomes. In fact, none was observed detached from IF in our samples. A fraction of the centrosomes (33%), on the other hand, was observed within the cytoplasm away from CK19 IF after incubation of the cells in acrylamide (Table I). Interestingly, this particular effect of acrylamide was almost

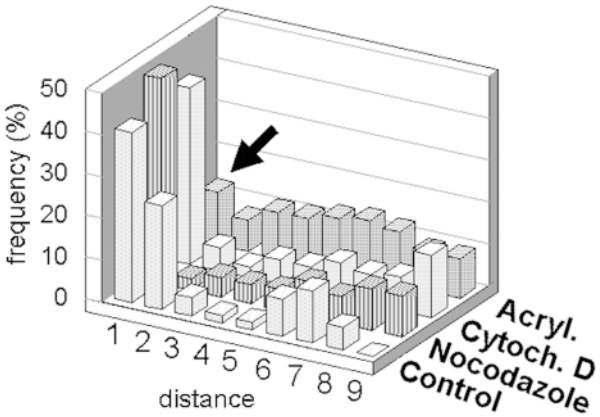

Figure 5. Separation of noncentrosomal γ-tubulin from CK19 IF induced by acrylamide but not by other anticytoskeletal agents. CACO-2 cells were grown on Transwell™ filters for 9 d. Before fixation, the monolayers were changed to DME supplemented with 33 μM nocodazole, 2 μM cytochalasin D (Cytoch. D), 5 mM acrylamide (Acryl.), or none (Control). The distance from noncentrosomal γ-tubulin spots to the nearest bundle of CK19 IF was measured in three-dimensional confocal deconvoluted images such as those shown in Fig. 2. The frequency of distances as percent, is shown for nine distance ranges: (1) <100 nm (below resolution), perfect colocalization as judged by this technique; (2) 100–300 nm, usually within the same confocal plane; (3) 300–600 nm; (4) 600–900 nm; (5) 900–1,200 nm; (6) 1,200–1,500 nm; (7) 1,500–1,800 nm; (8) 1,800–2,100 nm; (9) 2,100–2,400 nm. Most of the cases in the ranges 3–9 were distances measured in the z-axis. A total of 1,309 small γ-tubulin spots in 54 cells were counted, in approximately similar numbers for each treatment group. The 100% was considered as the total in each particular treatment. Notice that a large percent of the γ-tubulin colocalizes with apical IF in all treatments (~40%, range 1) except in cells treated with acrylamide (arrow).

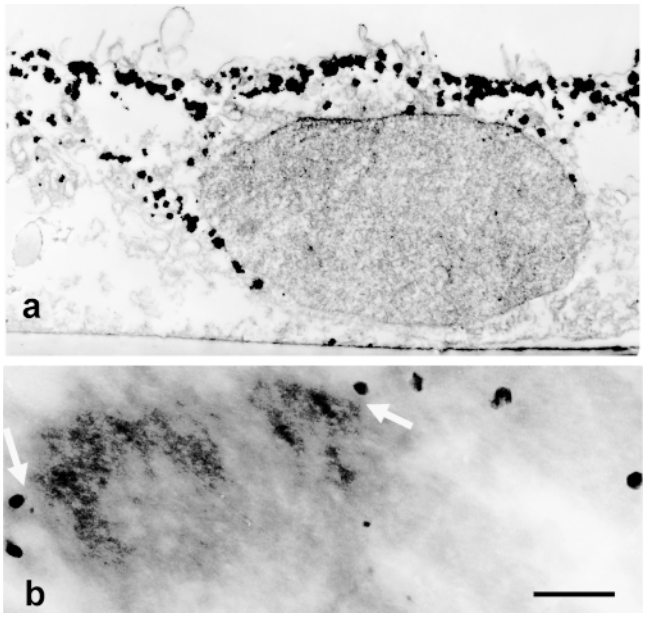

Figure 6. Colocalization of γ-tubulin and CK19 IF at EM level. CACO-2 cell monolayers were grown on filters as described above and fixed in methanol. CK19 was localized with Nanogold™ gold particles followed by silver developing, while γ-tubulin was localized using a standard immunoperoxidase procedure. (a) CK19-Nanogold™ signal was developed with silver for 20 min to attain 200–400 nm particles visible at low magnification. (b) The CK19-Nanogold™ signal was developed with silver for only 5 min, so that the particles were in the range 15–20 nm, and colocalized with γ-tubulin detected by immunoperoxidase (diffuse stain) reaction confined within a matrix of cross-linked albumin. Note that the minimum distance from gold particles to peroxidase stain is 10–20 nm (arrows). Bar: (a) 1.6 μm; (b) 0.1 μm.

completely reversible after 24 h (Table I). Likewise, a count of 1,309 noncentrosomal γ-tubulin spots in the apical-most 2.4 μm of the cytoplasm in cells subjected to treatment with anticytoskeletal agents showed no differences between control cells, and cells treated with nocodazole or cytochalasin D. In all three cases ~40% of the noncentrosomal γ-tubulin colocalized with IF (Fig. 5, distance range 1), and the treatments did not cause major changes in the distribution profile (Fig. 5, distance ranges 2–9). In cells treated with acrylamide, on the other hand, the percent of γ-tubulin spots decorating apical CK19 IF fell to <10% (Fig. 5, arrow). It is suggestive that the fraction of γ-tubulin colocalizing with IF is similar to the percent of insoluble γ-tubulin.

A similar study was attempted using colocalization experiments of γ-tubulin and CK18. Unfortunately, the tight codistribution of CK19 and CK18 IF in the apical cortical cytoskeleton made this analysis very difficult, as we cannot determine whether a spot of γ-tubulin signal in that region is attached to a bundle of CK19 IF or to a neighboring bundle of CK18 IF, or both. However, an analysis conducted on the relatively less common γ-tubulin signal attached to the extensions of CK18 IF under the lateral domain (Fig. 2 c) yielded an intriguing observation. In cells treated with acrylamide, the number of sparse γ-tubulin spots colocalizing with lateral CK18 IF did not change. Instead, only in cells treated with cytochalasin D we observed a dramatic decrease in the γ-tubulin decorating lateral CK18 IF. This result, a preliminary suggestion that attachment to both types of IF may be mediated by different mechanisms, will be further analyzed in the next section using coimmunoprecipitation procedures.

To analyze the codistribution of CK19 IF and γ-tubulin at the ultrastructural level, the former was localized with Nanogold, extremely small colloidal gold particles coupled to Fab affinity-purified anti–mouse IgG, that have extensive accessibility to antigens in cells fixed in toto. The size of gold particles was then increased with a silver enhancer that deposits around preexisting gold. To make them visible at low magnifications, the silver was allowed to deposit for 20 min, rendering particles of 200–400 nm. The apical distribution of CK19, with some extensions to the lateral domain that we reported before using immunoperoxidase (Salas et al., 1987) was fully confirmed. In addition, it was verified that, according to specifications, Nanogold particles can diffuse within fixed/permeabilized cytoplasms (Fig. 6 a, an extension of the signal along the lateral domain). For colocalization, γ-tubulin was localized using an immunoperoxidase reaction in cells embedded in cross-linked albumin, that restricts the diffusion of the diaminobenzidine product. Centrosome images were found in ~1 out of 30 cells in nonserial sections, always in the apical

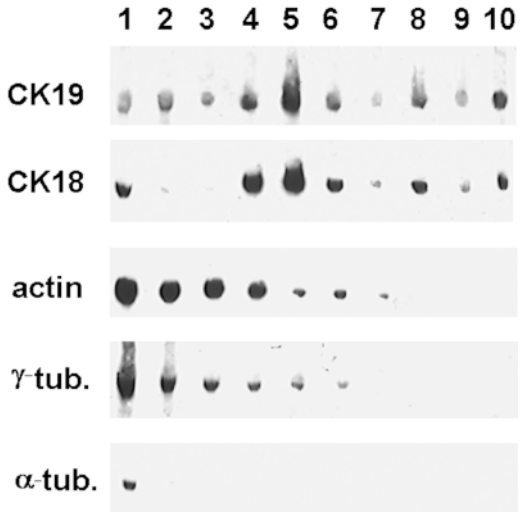

Figure 7. Distribution of cytoskeletal proteins from sonication fragments of cytoskeletal preparations of CACO-2 cells in sucrose gradients after velocity sedimentation. Cytoskeletal preparations of 9 d confluent CACO-2 monolayers were obtained by extraction in 1% Triton X-100, in EB-antiprotease cocktail. The cytoskeletons were extensively sonicated avoiding heating, and run in 20–60% sucrose gradients under rate centrifugation conditions to separate the fragments by size. Ten 1-ml fractions of the gradient were collected, diluted in PBS and pelleted (approximate sedimentation coefficient ranges per fraction: (1) 0–230S; (2) up to 430S; (3) up to 625S; (4) up to 790S; (5) up to 958S; (6) up to 1,100S; (7) up to 1,246S; (8) up to 1,376S; (9) up to 1,500S; and (10) up to 1,600S). The pellets were analyzed by SDS-PAGE and blotted onto nitrocellulose (fraction 1, top of the gradient). The same nitrocellulose sheet was sequentially probed, stripped off and reprobed with antibodies against CK19, CK18, actin, γ-tubulin (γ-tub.), and α-tubulin (α-tub). A second cycle of reprobing, and reprobing in a different sequence indicated that the differences were not due to protein loss after reprobing.

pole of the cells. The immunoperoxidase reaction for γ-tubulin was found, as expected, in the pericentriolar material, observed at high magnification (Fig. 6 b, diffuse stain). The diameters of the peroxidase-positive images were always <400 nm, indicating that the peroxidase reaction product had not significantly diffused beyond the boundaries of centrosomes. For colocalization, the silver enhancing of Nanogold was kept to 5 min, rendering particles in the 15–20-nm range. This CK19 signal was observed on filamentous material in the apical region around the centrosomes. The minimum gold particle-to-peroxidase signal distances was found to be ~10 nm (Fig. 6 b, arrows). Gold particles were never observed within the pericentriolar material nor peroxidase reaction product decorating filaments.

Native IF Fragments Coimmunoprecipitate with γ-Tubulin

Immunoprecipitation of CKs poses a challenge, since these proteins are highly insoluble when polymerized in IF. Standard methods of immunoprecipitation of CK involve denaturation in SDS/urea, followed by dilution in Triton, which are obviously not amenable to test coimmunoprecipitation. Instead, we have previously developed a technique to demonstrate coprecipitation of apical membrane proteins and IF (Rodriguez et al., 1984) by fragmenting Triton X-100 insoluble cytoskeletal preparations with extensive sonication under nondenaturing conditions. Sonication has been widely used to fragment filamentous structures such as nucleic acids (Eisner and Lindblad, 1989), actin microfilaments (Kinosian et al., 1993) or IF (Drochmans et al., 1978). Fragments with a random distribution of sizes are then separated by size by rate centrifugation in sucrose gradients. 10 fractions of one of these gradients were analyzed by immunoblot for their content in various cytoskeletal components. Cytoskeletal fragments of CACO-2 cells containing CK18 and CK19 were present in nearly all fractions. Actin was present in fractions 1–7 and α-tubulin only in the top fraction (Fig. 7). The latter result was expected since the extraction in the cold was not devised to preserve microtubules. Interestingly, the γ-tubulin signal extended to the 6th fraction (approximately up to 1,100 S). This distribution in a gradient of insoluble γ-tubulin contrasts with that of soluble γ-tubulin complexes that are typically 28 S.

To further analyze possible binding of γ-tubulin containing structures to IF, the fractions from this type of gradient were immunoprecipitated with a polyclonal antibody against the COOH-terminal region of γ-tubulin. The immunoprecipitates were analyzed sequentially by immunoblot using a monoclonal antibody anti-CK19 (Fig. 8, top immunoblot panels), and then by stripping off the first set of antibodies and reprobing the same nitrocellulose sheets with an antibody against CK18 (Fig. 8, second row of immunoblot panels). It should be noticed that the order of reprobing did not affect the results, as described in Fig. 7. The immunoprecipitation was carefully controlled in parallel aliquots with a nonimmune rabbit IgG (Fig. 8, −). It was early noted that nonspecific precipitation increased from none in the first three fractions, to very significant levels in the bottom of the gradient, presumably because very large fragments of the cytoskeleton pellet together with the agarose beads. Therefore, we restricted our analysis to the top five fractions of the gradients where the specific, antibody-dependent signal was clearly larger than nonspecific precipitation (Fig 8, + lanes versus − lanes). To compare these data with the previous results using anticytoskeletal agents, some monolayers were also treated with nocodazole, acrylamide, or cytochalasin D at the same concentrations and times described in Table I, before Triton extraction. In control monolayers, CK19 coimmunoprecipitated with γ-tubulin in the top 5 fractions of the gradient. Interestingly, when the same immunoprecipitates were analyzed for CK18, only the top 1 or 2 fractions were reactive (Fig. 8), even when CK18 was abundantly present in fractions 4 and 5 as well (Fig. 7). This result strongly supports the notion that insoluble γ-tubulin–containing structures are bound to IF. An extensive treatment with nocodazole (7 h) did not affect the coimmunoprecipitation with CK19 or CK18. The acrylamide treatment, on the other hand, erased the specific coimmunoprecipitation with CK19, but not the coimmunoprecipitation with CK18. Conversely, the cytochalasin D treatment abolished coimmunoprecipitation with CK18, while CK19 was still present in the same immunoprecipitates (Fig. 8). These results correlate well with the morphological colocalization data described in

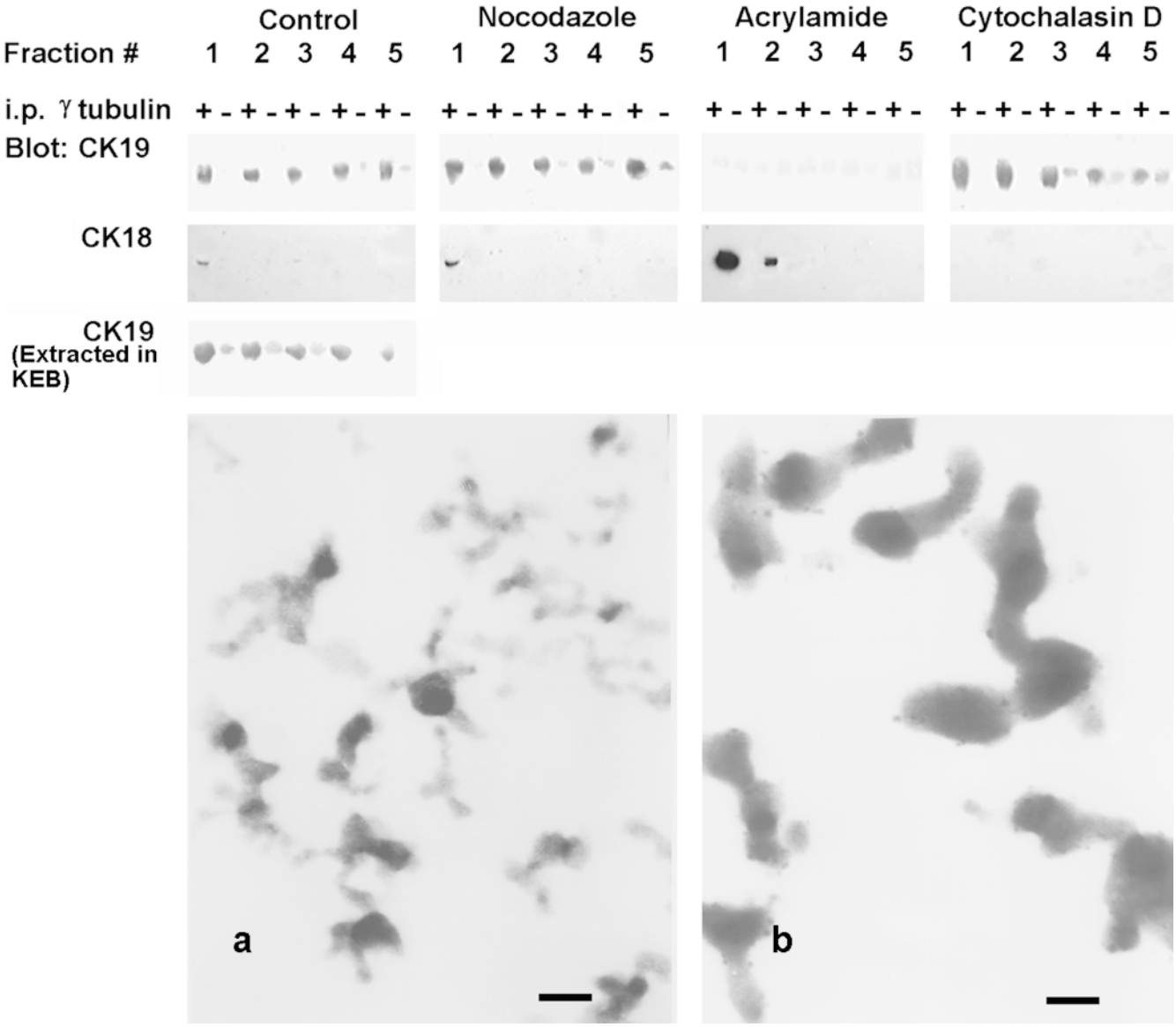

Figure 8. Coimmunoprecipitation of CK19 and CK18 with γ-tubulin from native cytoskeletal fragments obtained by sonication and separated in sucrose gradients, are sensitive to acrylamide and cytochalasin D, respectively. CACO-2 cell monolayers were grown for 9 d on Transwell™ filters, and treated with anticytoskeletal agents as described in Fig. 5 before detergent extraction. Sonication fragments of cytoskeletal preparations were obtained and separated as described in Fig. 7, with the exception of the bottom immunoblot panel, obtained from samples extracted in a physiologic (KEB) buffer, in the presence of saponin, antiproteases, and phosphatase inhibitors. Each one of the top five fractions (containing fragments in the range 0–510 S) was diluted, divided in two equal aliquots, and subjected to immunoprecipitation with anti–γ-tubulin antibody (+) or with nonimmune purified rabbit IgG at an equivalent concentration (−). After extensive washes, the protein A–agarose beads were eluted in SDS-urea, the eluates were TCA precipitated, run in SDS-PAGE, and blotted. The same nitrocellulose sheets were sequentially probed, stripped off, and reprobed with anti-CK19 mAb and with anti-CK18 mAb. (Bottom panels) Electron microscopy of the cytoskeletal fragments in fractions 1 (a) and 5 (b). Samples from the same gradients, before immunoprecipitation, were fixed in glutaraldehyde, pelleted, embedded, sectioned, and stained for TEM. Bars, 60 nm.

the previous section, and suggest that γ-tubulin–containing structures bind to CK18 and CK19 IF via two different mechanisms, one cytochalasin D sensitive (perhaps mediated by actin) and the other acrylamide sensitive. Because there is always the possibility that binding between two structures may be artefactually induced during detergent extraction, a control was done changing the extraction buffer to a different more physiological buffer (KEB), replacing Triton X-100 by 0.1% saponin, that permeabilizes membranes but does not extract material, and adding a cocktail of phosphatase inhibitors in addition to the protease inhibitors. Coimmunoprecipitation of CK19 with γ-tubulin was observed again in sonication fragments obtained under these milder extraction conditions. However, as expected from a preparation that now contained membranes, the distribution of the specific signal in the gradient was different than in the Triton X-100 fragments (Fig. 8, bottom immunoblot panel).

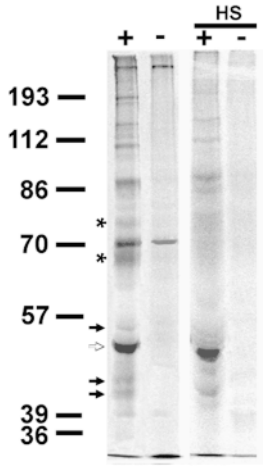

Figure 9. Protein composition of the complexes immunoprecipitated with anti–γ-tubulin antibody. CACO-2 cell monolayers (7.5 × 107 cells) were metabolically labeled with [^{35}S]methionine-cysteine for 24 h, extracted, sonicated, and pools of fractions 1 and 2 were immunoprecipitated (+, anti–γ-tubulin antibody; −, nonimmune rabbit IgG) as described above. An equivalent amount of immunoprecipitate still bound to the beads was washed in EB supplemented with 0.7 M NaCl (HS). The eluates were analyzed by SDS-PAGE and autoradiogram. Molecular mass standards are expressed in kD.

To control the possibility that the co-i.p. may be due to simple physical trapping of insoluble γ-tubulin into IF meshworks or cages, we analyzed the cytoskeletal fragments in the gradients under EM. In fraction 1 the fragments were fibrous, with an average caliper diameter of 30 nm and length of 105 nm (Fig. 8 a). Only in a few fields small granule-like structures were seen (not shown). In fraction 5, the vast majority of the fragments were rod-like, with an average caliper diameter of 49 nm and average length of 180 nm (Fig 8 b). Similar results were observed in the material spread on carbon-coated grids (not shown). No meshwork-like structures were observed at all. Clearly, the size and simple geometry of these fragments cannot sustain physical trapping of much larger (∼300 nm) centrosomes.

Next, the composition of the multi-protein complexes in which γ-tubulin and CK19 coimmunoprecipitate was analyzed by metabolic labeling with [^{35}S]methionine/cysteine for 24 h. Sonication fragments of the cytoskeletal preparation were separated in sucrose gradients and pools of the top two fractions were immunoprecipitated with anti–γ-tubulin antibody. The autoradiograms showed z10 antibody-specific bands and 3 unspecific bands (Fig. 9). The lower four specific bands had been identified in immunoblot as CK8, CK18, and CK19 (Fig. 9, black arrows, from top to bottom). The dense 50-kD band corresponded to γ-tubulin (Fig. 9, white arrow). There were still approximately six unidentified peptides in the complexes. To distinguish which ones belong to the MTOC, a parallel set immunoprecipitates, still bound to the beads, was washed for 2 h in EB supplemented with 0.7 M NaCl, a condition known to disassemble soluble γ-tubulin complexes (Stearns and Kirshner, 1994) but not IF-associated proteins. The unspecific bands and two of the specific bands (67 and 76 kD, Fig. 9, HS, *) disappeared from these preparations, suggesting that the remaining four specific polypeptides (90, 105, 110, and 180 kD) may be IF-associated proteins or part of the insoluble scaffold that holds γ-tubulin.

Discussion

To test the hypothesis that γ-tubulin–containing structures are attached to IF under the apical pole of epithelial cells we have used three independent approaches: morphological colocalization, analysis of the effect of antisense down-regulation of CK19 on centrosome localization, and coimmunoprecipitation in multiprotein cytoskeletal fragments obtained under nondenaturing conditions. Each one of these techniques has advantages and potential problems. The data of the three approaches, however, is complementary and consistent with the notion that centrosomes and a substantial fraction of noncentrosomal γ-tubulin containing structures bind to apical IF.

Colocalization of γ-Tubulin with Intermediate Filaments

The largest of the γ-tubulin structures were easily identified as centrosomes. All the noncentrosomal γ-tubulin signal was observed in discrete spot-like images. It should be noted that, because these images are the result of indirect immunofluorescence, they represent a slight overestimation of the real size. In fact, given the Stokes radius of the IgG (∼7 nm) in the two layers of antibody covering a structure, one should add a total of ∼28 nm to the original diameter of the structure. The smaller noncentrosomal spots, therefore, after subtracting the contribution of the IgG must be ∼140 nm in diameter and are difficult to identify with previously described structures. This diameter represents nearly five times the diameter of the ring-shaped soluble γ-tubulin complexes described by Zheng et al. (1995). However, because these structures are at the limit of resolution of our instrument, they must be considered as points without any further estimation of their real size. Furthermore, neither of our anti–γ-tubulin antibodies recognized the epitope in aldehyde fixed cells, and were amenable to use only under methanol fixation, so that I cannot be sure if this discrete γ-tubulin signal is a fixation artefact. Therefore, I am not drawing any conclusion about the structure of noncentrosomal γ-tubulin signal, except that its localization in the apical pole of epithelial cells is consistent with the localization of noncentrosomal MTOC described by others (Meads and Schroer, 1995).

Resolution of scanning laser confocal microscopy coupled to appropriate deconvolution analysis of three-dimensional images has been proven to yield resolutions at or below the 100-nm level in the XY plane (Rizzuto et al., 1998). Deconvolution processes can yield sub-pixel resolution, even for standard (nonlaser) epi-illumination (Carrington et al., 1995). We experimentally verified this fact in our system, together with the coalignment of the channels using fluorescent beads. The resolution in the z-axis, on the other hand, was slightly less reliable, and we experimentally verified it at ∼300 nm. It must be noted that the colocalization of centrosomes and noncentrosomal γ-tubulin with IF at this level of resolution is more accurate than most colocalizations reported in the literature with standard epifluorescence microscopy, where resolution is 250 nm at best. It can be argued that IF in the apical network are very crowded and that any structure in the same region will randomly touch an IF bundle. While this may be true for centrosomes due to their size, this argument is unsustainable for noncentrosomal γ-tubulin. The surface occupied by IF signal at any XY confocal section is <50% of the image, and the gaps are significantly larger than the noncentrosomal γ-tubulin spots (Fig. 2, d and e, small arrows). Yet,

<10% of the γ-tubulin signal was not in direct contact with CK signal, indicating a high degree of colocalization. In the case of centrosomes, there was also a perfect colocalization in the z-axis within the ~1 μm thickness of the apical IF network. Considering that differentiated CACO-2 cells grown on filters are 10–20 μm tall, the position of centrosomes exactly at the level of the apical IF network can be considered a bona fide colocalization. The colocalization with F-actin with γ-tubulin, on the other hand, was good in the lateral domain, but poor in the terminal web, a result consistent with the possibility that different mechanisms of anchoring operate at different domains.

Additional evidence was provided by colocalization experiments at the EM level. While there is consensus in the precision of the localization with gold particles, some concerns may arise in regards to the peroxidase/diaminobenzidine reaction product that, potentially, may diffuse away from the site of the antigen. This diffusion can be efficiently confined within ~10 nm of the site of the antigen by performing the peroxidase reaction within a matrix of glutaraldehyde cross-linked albumin as described by Brown and Farquhar (1984), and also shown for membrane proteins (Vega-Salas et al., 1987b). Given this possible margin of error and the size of the gold particles themselves, the minimum distance between CK19 and γ-tubulin may be in the range of 10–20 nm. Because no overlapping of signals was observed, the binding interface between centrosomes and IF may be located at the outer boundary of the pericentriolar material (as labeled by γ-tubulin). In addition, it is possible that one or more intermediary proteins may be intercalated between CKs and γ-tubulin.

To our knowledge, this is the first report of colocalization of γ-tubulin with cytokeratin IF. Trevor et al. (1995), however, have reported colocalization of centrosomes with vimentin IF in cells that normally do not express IF, transfected with a vimentin-expressing vector, suggesting that this may be a more general function of IF.

Coimmunoprecipitation of γ-Tubulin–containing Structures with CK Intermediate Filaments

In general, coimmunoprecipitation is accepted as evidence of binding between two proteins. In this case, however, we attempted the difficult task of analyzing the protein interactions of the ~50% of γ-tubulin that is insoluble (Stearns and Kirschner, 1994) and has not been previously characterized. To avoid denaturing conditions, we resorted, as in a previous publication (Rodriguez et al., 1994), to a fine homogenization of the Triton insoluble cytoskeletal preparation by sonication that yields multi-protein fragments. To apply this method for immunoprecipitation purposes we faced the limitation that the largest fragments (fractions 6–10 in our gradients) are heavy enough to pellet together with the agarose beads. Our original approach to this problem was to separate the beads from the unbound fragments by filtration through a 15-μm nylon mesh. Although this method successfully washes the beads, it has been our experience that, during the backwash of the filter, to recover the specific signal, sometimes there is loss of material, presumably beads retained in the filter or the filter holder. To avoid this and to ensure that the results would enable us to compare gradients from monolayers under different treatments, we decided to study only those fractions (1–5) that were amenable for standard immunoprecipitation, and to do so with careful parallel controls for nonspecific precipitation (Figs. 8 and 9, − lanes). The results indicate that we were able to precipitate multi-protein complexes in a specific antibody-dependent fashion, and which contained insoluble γ-tubulin and also either CK19 or CK18.

Interestingly, the results indicate that the complexes of γ-tubulin with the two types of IF were different in their migration in the gradient and their stability after treatments with anticytoskeletal agents. The CK19–γ-tubulin complexes displayed a broader range of sizes and were sensitive to pretreatment of the cells with acrylamide, while the CK18–γ-tubulin complexes were smaller, and sensitive only to pretreatment with cytochalasin D. These data are consistent with the morphological results (Fig. 5 and Table I) and suggest the possibility that MTOC may be bound to CK18 and CK19 via different mechanisms.

Because we were immunoprecipitating fragments of the cytoskeletal preparation or naturally occurring discrete particles, and not soluble proteins, careful thought has to be given to the possibility that Triton insoluble γ-tubulin–containing structures may be physically trapped within IF networks. An obvious prediction of a caging model is that structures of similar sizes, from the same domain must be caged together. If the CK19 cages can physically trap 300-nm centrosomes, they should also trap bundles of CK18-8 IF, especially since both sets of bundles are closely intermingled in the apical network. This was not the case in our experiments. If the γ-tubulin containing structures were physically trapped in fractions 2–5 of the gradients, it is inconceivable that no CK18 IF were trapped in the same cages (Fig. 8), even in the relatively large fragments of fractions 4 and 5. It must be remembered that CK18 was present in fractions 4 and 5 of the gradient before the immunoprecipitation (Fig. 7). In fact, the different behavior of CK18 and CK19 coimmunoprecipitation with γ-tubulin should lead us to conclude that two perfectly distinct sets of cages were generated by sonication: a small one (fractions 1 and 2) made of CK18 IF that can be opened with cytochalasin D but not with acrylamide, and another one, of a wider range of sizes made only of CK19 IF, sensitive to acrylamide but not to cytochalasin D. Such an exquisite specificity seems extremely unlikely for randomly generated three-dimensional lattices trapping structures inside.

A second line of experimental evidence against physical trapping comes from the visualization of the cytoskeletal fragments separated by the gradient under EM (Fig. 8, a and b). No evidence of three-dimensional lattices capable of trapping centrosomes was found. The structure of insoluble γ-tubulin is unknown and it has been tentatively equated to that associated with centrosomes (Stearns and Kirschner, 1994). There is a possibility, however, that a fraction of the rather abundant noncentrosomal γ-tubulin may also be found in the insoluble cytoskeletal preparation. One can only speculate that the structure of this putative noncentrosomal insoluble γ-tubulin may be similar to that of the ring-like γ-tubulin particles (Zheng et al., 1995) in the soluble fraction, or, perhaps a multimer of them. In this regard, it is unlikely that the noncentrosomal γ-tubulin exists in pieces smaller than 28 nm. In this scenario, there-

fore, it is also unlikely that 40–50 nm fragments of the cytoskeleton in fraction 1 can sustain physical trapping of 28 nm (or bigger) γ-tubulin complexes or vice versa. Finally, because coimmunoprecipitation was also observed under totally different, more physiological, extraction conditions in the presence of phosphatase blockers (Fig. 8, KEB), and resistant to high salt (Fig. 9), we believe that an artefactual attachment of IF to MTOC due to detergent extraction is also very unlikely. On this basis, the coimmunoprecipitation results indicate that there is binding of γ-tubulin and cytokeratins to the same multiprotein complexes.

These complexes comprised γ-tubulin, the CKs, and about six other unidentified proteins. γ-tubulin was clearly more abundant than CK8 (Fig. 9), a result that suggests that some of the MTOC fragments, not associated with IF, are also being immunoprecipitated. However, it must be noted that CKs display turnovers of 100 h or more (Denk et al., 1987). Therefore, the 24 h labeling may be tagging 30% or less of the CKs. Two of the other proteins disassembled from the complexes in high salt buffer while the association with CKs was maintained. Because of the complex nature of the MTOC (Archer and Solomon, 1994), this suggests that the sonication fragments contain only part of the MTOC, perhaps corresponding to the outer boundary of the pericentriolar region. The remaining five proteins were resistant to high salt extraction. Any of these proteins may be intermediaries in the attachment of γ-tubulin to IF, or alternatively the binding between γ-tubulin and CKs may be direct. Further research is necessary to establish the architecture of the protein-protein interactions at the centrosome–IF interface.

Effect of CK19 Downregulation by Antisense Oligonucleotide on the Localization of Centrosomes

The effects of anti-CK19 antisense phosphorothioate oligodeoxy nucleotides on the polarity and cytoskeletal organization of CACO-2 cells have been documented before (Salas et al., 1997). Here we used the antisense-mediated downregulation of CK19 to analyze the effects of tampering with the subpopulation of IF that are specifically apical on the localization of potential MTOC. It should be noted that we and others (Noonberg et al., 1993) determined that the uptake of oligonucleotides decreases as the monolayer becomes confluent, thus providing a possible explanation of why the effect is transitory and heterogeneous. A relatively narrow time window to observe the effects in well differentiated CACO-2 cells, around 9 d after seeding, was previously determined. We took advantage of this fact, however, by using the nontargeted cells as an internal control for the distribution of centrosomes. The heterogeneity in the effect may arise from the decreased uptake of oligonucleotides after the monolayers become confluent (Salas et al., 1997). Additional controls were provided by cells subjected to identical treatment with oligonucleotides with the same bases, in a randomized sequence, synthesized at the same time and with the same reagents as the antisense. In contrast with control cells, >60% of the cells downregulated in CK19 showed centrosomes either totally disconnected from the cortical region or on the lateral domain.

It is important to highlight that, in the 36% of the partially targeted cells, where centrosomes were still in their normal position, there was always a perfect colocalization with one remnant CK19 bundle of IF. We have extensively documented that these cells have their normal content and localization of CK18 IF. Therefore, it can be concluded that CK19 IF can successfully compete with a large excess of CK18 IF to bind the centrosomes.

It can be argued that CK19 downregulation may cause indirect catastrophic effects on other components of the cytoskeleton. We have previously characterized those effects. The most striking consequence of CK19 downregulation is the loss of apical F-actin, while lateral cortical actin and basal stress fibers remain undisturbed (Salas et al., 1997). If the effects of CK19 downregulation on the localization of centrosomes were a consequence of the disruption of the apical F-actin, they should be mimicked by cytochalasin D, which was obviously not the case. Second, downregulation of CK19 also induces a slight redistribution of the apical microtubule network. Again, if this effect was responsible for the displacement of centrosomes, it would have been mimicked by nocodazole either with the morphological or biochemical analyses.

In summary, three independent methods showed that the apical IF bind centrosomes and a fraction of the noncentrosomal γ-tubulin. Given the well established role of γ-tubulin in the organization of MTOC, it seems safe to conclude that part of all this insoluble γ-tubulin must represent the MTOC that predictably exist in the apical domain of epithelial cells. This as yet unsuspected interaction between IF and MTOC may yield a better explanation of how the cytoskeleton is organized, and warrants the need for future investigations in search for the molecular basis of the MTOC-IF binding.

I am deeply thankful to Drs. Fulvia Verde (Department of Biochemistry and Molecular Biology) and Richard Rotundo for critically reading the manuscript. I would like to thank Ms. Yolanda Figueroa and Susan Decker for technical assistance.

This work was supported by a grant from National Institutes of Health (K14HL03397-01).

Submitted: 15 December 1998
Revised: 28 June 1999
Accepted: 8 July 1999

References

Apodaca, G., L.A. Katz, and K.E. Mostov. 1994. Receptor-mediated transcytosis of IgA in MDCK cells is via apical recycling endosomes. *J. Cell Biol.* 125: 67–86.

Archer, J., and F. Solomon. 1994. Deconstructing the microtubule-organizing center. *Cell.* 76:589–591.

Bacallao, R., C. Antony, C. Dotti, E. Karsenti, E.H.K. Stelzer, and K. Simons. 1989. The subcellular organization of Madin-Darby Canine kidney cells during the formation of a polarized epithelium. *J. Cell Biol.* 109:2817–2832.

Brown, W.J., and M.G. Farquhar. 1984. The mannose-6-phosphate receptor for lysosomal enzymes is concentrated in Cis Golgi cisternae. *Cell.* 36:295–307.

Buendia, B., M.H. Bré, G. Griffiths, and E. Karsenti. 1990. Cytoskeletal control of centrioles movement during the establishment of polarity in MDCK cells. *J. Cell Biol.* 110:1123–1135.

Denk, H., E. Lackinger, K. Zatloukal, and W.W. Franke. 1987. Turnover of cytokeratin polypeptide in mouse hepatocytes. *Exp. Cell Res.* 173:137–143.

Eckert, B.S. 1986. Alteration of the distribution of intermediate filaments in PtK1 cells by acrylamide. II: effect on the organization of cytoplasmic organelles. *Cell Motil. Cytoskel.* 6:15–24.

Elsner, H.I., and E.B. Lindblad. 1989. Ultrasonic degradation of DNA. *DNA.* 8:697–701.

Grindstaff, K.K., R.L. Bacallao, and W.J. Nelson. 1998. Apiconuclear organization of microtubules does not specify protein delivery from the trans-Golgi

network to different membrane domains in polarized epithelial cells. *Mol. Biol. Cell.* 9:685–699.

Kinosian, H.J., L.A. Selden, J.E. Estes, and L.C. Gershman. 1993. Actin filament annealing in the presence of ATP and phalloidin. *Biochemistry*. 32: 12353–12357.

Laemmli, U.K. 1970. Cleavage of structural proteins during the assembly of bacteriophage T4. *Nature.* 227:680–685.

Lafont, F., J.K. Burkhardt, and K. Simons. 1994. Involvement of microtubule motors in basolateral and apical transport in kidney cells. *Nature.* 372:801–803.

Luby-Phelps, K., P.E. Castle, D.L. Taylor, and F. Lanni. 1987. Hindered diffusion of inert tracer particles in the cytoplasm of mouse 3T3 cells. *Proc. Natl. Acad. Sci. USA*. 84:4910–4913.

Meads, T., and T.A. Schroer. 1995. Polarity and nucleation of microtubules in polarized epithelial cells. *Cell Motil. Cytoskel.* 32:273–288.

Mostov, K.E. 1995. Regulation of protein traffic in polarized epithelial cells. *Bioessays.* 17:129–138.

Noonberg, S.B., M.R. Garovoy, and C.A. Hunt. 1993. Characteristics of oligonucleotide uptake in human keratinocyte cultures. *J. Invest. Dermatol.* 101: 727–731.

Oakley, B.R., C.E. Oakley, Y. Yoon, and M.K. Jung. γ-Tubulin is a component of the spindle pole body that is essential for microtubule function in *Aspergillus nidulans. Cell.* 61:1289–1301.

O'Farrell, P.H. 1975. High resolution two-dimensional electrophoresis of proteins. *J. Biol. Chem*. 250:4007–4021.

Redenbach, D.M., and A.W. Vogl. 1991. Microtubule polarity in Sertoli cells: A model for microtubule-based spermatid transport. *Eur. J. Cell Biol.* 54:277–290.

Reinsch, S., and E. Karsenti. 1994. Orientation of spindle axis and distribution of plasma membrane proteins during cell division in polarized MDCKII cells. *J. Cell Biol.* 126:1509–1526.

Rizzolo, L.J., and H.C. Joshi. 1993. Apical orientation of the microtubule organizing center and associated gamma-tubulin during the polarization of the retinal pigment epithelium in vivo. *Dev. Biol.* 157:147–156.

Rodriguez-Boulan, E., and W.J. Nelson. 1989. Morphogenesis of the polarized epithelial cell phenotype. *Science.* 245:718–725.

Rodriguez, M.L., M. Brignoni, and P.J.I. Salas. 1994. A specifically apical submembrane intermediate filament cytoskeleton in non-brush-border epithelial cells. *J. Cell Sci.* 107:3145–3151.

Salas, P.J.I., M.L. Rodriguez, A. Viciana, D.E. Vega-Salas, and H.P. Hauri. 1997. The apical sub-membrane cytoskeleton participates in the organization of the apical pole in epithelial cells. *J. Cell Biol.* 137:359–375.

Salas, P.J.I., D.E. Vega-Salas, J. Hochman, E. Rodriguez-Boulan, and M. Edidin. 1988. Selective anchoring in the specific plasma membrane domain: a role in epithelial cell polarity. *J. Cell Biol.* 107:2363–2376.

Shabana, A.H.M., M. Oboeuf, and N. Forest. 1994. Cytoplasmic desmosome and intermediate filament disturbance following acrylamide treatment in cultured rat keratinocytes. *Tissue Cell.* 26:43–55.

Simons, K., and A. Wandinger-Ness. 1990. Polarized sorting in epithelia. *Cell.* 62:207–210.

Stearns, T., and M. Kirschner. 1994. In vitro reconstitution of centrosome assembly and function: the central role of γ-tubulin. *Cell.* 76:623–637.

Stearns, T., L. Evans, and M. Kirschner. 1991. γ-Tubulin is a highly conserved component of the centrosome. *Cell.* 65:825–836.

Steinert, P., R. Zackroff, M. Aynardi-Whitman, and R.D. Goldman. 1982. Isolation and characterization of intermediate filaments. *Methods Cell Biol.* 24: 399–419.

Trevor, K.T., J.G. McGuire, and E.V. Leonova. 1995. Association of vimentin intermediate filaments with the centrosome. *J. Cell Sci.* 108:343–356.

Trout, L.L., and B. Burnside. 1988. The unusual microtubule polarity in teleost retinal pigment epithelial cells. *J. Cell Biol.* 107:1461–1464.

Vega-Salas, D.E., P.J.I. Salas, D. Gundersen, M. Cereijido, and E. Rodriguez-Boulan. 1987a. Formation of the apical pole of epithelial (Madin-Darby canine kidney) cells: polarity of an apical protein is independent of tight-junctions while segregation of a basolateral marker requires cell-cell interactions. *J. Cell Biol.* 104:905–916.

Vega-Salas, D.E., P.J.I. Salas, and E. Rodriguez-Boulan. 1987b. Modulation of the expression of an apical plasma membrane protein of Madin-Darby canine kidney epithelial cells. Cell-cell interactions control the appearance of a novel intracellular storage compartment. *J. Cell Biol.* 104:1249–1259.

Wollner, D.A., and W.J. Nelson. 1992. Establishing and maintaining epithelial cell polarity. Roles of protein sorting, delivery and retention. *J. Cell Sci.* 102: 185–190.

Zheng, Y., M.L. Wong, B. Alberts, and T. Mitchison. 1995. Nucleation of microtubule assembly by a γ-tubulin-containing ring complex. *Nature.* 378:578–583.